View Article Online
View Journal

Journal of Materials Chemistry A

Accepted Manuscript

This article can be cited before page numbers have been issued, to do this please use: L. sun, Y. Yun, H. Sheng, Y. Du, Y. Ding, P. Wu, P. li and M. Zhu, *J. Mater. Chem. A*, 2018, DOI: 10.1039/C8TA04667K.

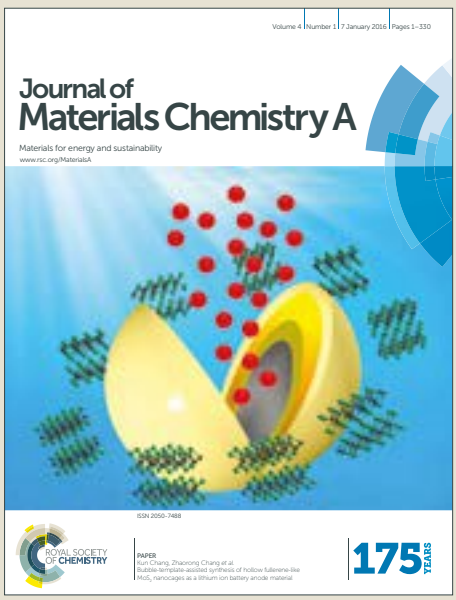

This is an Accepted Manuscript, which has been through the Royal Society of Chemistry peer review process and has been accepted for publication.

Accepted Manuscripts are published online shortly after acceptance, before technical editing, formatting and proof reading. Using this free service, authors can make their results available to the community, in citable form, before we publish the edited article. We will replace this Accepted Manuscript with the edited and formatted Advance Article as soon as it is available.

You can find more information about Accepted Manuscripts in the author guidelines.

Please note that technical editing may introduce minor changes to the text and/or graphics, which may alter content. The journal's standard Terms & Conditions and the ethical guidelines, outlined in our author and reviewer resource centre, still apply. In no event shall the Royal Society of Chemistry be held responsible for any errors or omissions in this Accepted Manuscript or any consequences arising from the use of any information it contains.

ROYAL SOCIETY OF CHEMISTRY

rsc.li/materials-a

View Article Online
DOI: 10.1039/C8TA04667K

Journal Name

COMMUNICATION

Rational Encapsulation of Atomically Precise Nanoclusters into Metal-Organic Frameworks by Electrostatic Attraction for CO_2 Conversion

Received 00th January 20xx,
Accepted 00th January 20xx

DOI: 10.1039/x0xx00000x

www.rsc.org/

Lili Sun,† Yapei Yun,† Hongting Sheng,* Yuanxin Du, Yimin Ding, Pei Wu, Peng Li, Manzhou Zhu*

Controlled encapsulation of atomically precise nanoclusters (APNCs) into metal organic frameworks (MOFs) has been an efficient way to create new types of multifunctional crystalline porous materials. Such hybrids (APNCs@MOFs) provide ideal candidates for studying of inherent structure-catalysis relationships owing to their well-defined compositions of both components. Moreover, modeling on APNCs@MOFs with precise structures would be more reliable. Herein, we have established an "Electrostatic Attraction Strategy" to synthesize APNCs@MOFs catalysts and studied their performance as catalysts for the conversion of CO_2. The synthetic strategy presented here has been proved to general, evidenced by the syntheses of various APNCs@MOFs catalysts including all the combinations of $[Au_{12}Ag_{32}(SR)_{30}]^{4-}$, $[Ag_{44}(SR)_{30}]^{4-}$, $[Ag_{12}Cu_{28}(SR)_{30}]^{4-}$ nanoclusters with ZIF-8, ZIF-67, MHCF frameworks. Specifically, the as-obtained $Au_{12}Ag_{32}(SR)_{30}$@ZIF-8 composite shows excellent performance in capturing CO_2 and converting phenylacetylene into phenylpropiolate under mild conditions (50°C and ambient CO_2 pressure) with a TON as high as 18164, far exceeding those of most known catalysts. What's more, the catalyst is very stable and reused for 5 times without loss of catalytic activity. We anticipate that this general synthetic approach may open up a new frontier in the development of promising APNCs@MOFs catalysts, which can be applied in a broad range of heterogeneous catalysis in the future.

Introduction

Recently metal–organic frameworks (MOFs) have attracted extensive interest and stand out in a variety of applications, especially in catalysis, because of their tailorability and diversity.[1-5] However, the categories of active sites in MOFs are mainly restricted to the acid (or base) sites of unsaturated metal nodes and organic linkers.[3,6-10] Employing the permanent porosity of MOF, combining with functional guest species and MOF yields a synergistic effect for boosting catalytic performance and/or expanding the range of reactions.[3] Herewith, extensive efforts have been made to fabricate composites of MNPs@MOFs (MNPs: metal nanoparticles), which exhibited excellent catalytic activities owing to the confinement effect preventing MNPs from growing during the catalysis.[11-15] However, the clarification of detailed mechanism over these MNPs@MOFs composites is seriously hampered by the unclear structure of MNPs.[11-13] APNCs with precise structures enable understanding the relationship between the structure and properties at atomic level. Rational encapsulation of APNCs into MOFs is an efficient way to create a promising multifunctional porous material with well-defined structures of both components. The above idea was also explicitly put forward in the outlook of a latest review on MOFs.[1]

Previously our group has reported the preparation of monodisperse Au NCs supported on MOFs by an in-situ chemical reduction method, including the $Au_{11}(PPh_3)_8Cl_2$@ZIF-8 and $Au_{13}Ag_{12}(PPh_3)_{10}Cl_8$@MIL-101 composites.[16] However, the in-situ chemical reduction method for APNCs@MOFs composites has two shortcomings. First, it is difficult to encapsulate all APNCs in the framework of the MOF by in-situ reduction so far. There are always some APNCs deposited on the outer surface of MOF. When the composites were washed by methylene chloride, some APNCs were detached from the surface of MOFs, which resulted in poor recycling ability of the composites during the catalytic process. Second, the method is poorly controllable. This makes it difficult for designing and regulating the structure of APNCs, which is bad for adjusting APNC structure in elucidating structure-activity relationship. Therefore, there is a critical need for well-designed APNCs@MOFs nanomaterials and facile synthetic methods for such materials.

Rosi *et al*. published a cation exchange method, which can successfully encapsulated a pre-synthesized nanocluster $Au_{133}(SR)_{52}$ into the MOF-102/106 crystal. However, the cation exchange method requires H_2O_2 oxidant to pretreat Au

*Department of Chemistry and Center for Atomic Engineering of Advanced Materials, Anhui University, Hefei, Anhui 230601, China. *E-mail: sht_anda@126.com; zmz@ahu.edu.cn*
† L. Sun and Y. Yun contributed equally.
Electronic Supplementary Information (ESI) available.

nanoclusters in order to promote cation exchange-driven diffusion.[17] Recently, another new "coordination-assisted self-assembly" method has been established to synthesize $Au_{25}(SG)_{18}$@ZIF-8 (SGH = glutathione), which is like the "bottle-around-ship" technique of the Zn^{2+} ions coordination with the carboxyl group in the GS-ligand of Au_{25} NCs, lead to ZIF-8 growing surround the pre-synthesized $Au_{25}(SG)_{18}$ cores[18]. Whereas, the majority of well-defined APNCs are oil-soluble nanoclusters with various thiol ligands. To sum up, there is a urgent need to develop an simple and effective strategy for rational encapsulation of such thiol-protected APNCs into MOFs as highlighted contributions.

Electrostatic self-assembly is a well-established strategy to create well-mixed nanocomposites.[19-21] It is the principle of using oppositely charged species to attract each other. Based on this strategy, we envision that it would be crucial that introducing oil-soluble anionic APNCs for subsequent MOFs growth under mild conditions by electrostatic attraction between anionic APNCs and cationic metal ions of MOFs. In the current work, this strategy is demonstrated to be very successful, in which anionic $[Au_{12}Ag_{32}(SR)_{30}]^{4-}$ nanoclusters[22] are encapsulated with good dispersity and fully confined inside ZIF-8,[23] ZIF-67[24] and MHCF,[25] respectively. More importantly, the method is also valid for various anionic nanoclusters such as $[Ag_{44}(SR)_{30}]^{4-}$ and $[Ag_{12}Cu_{28}(SR)_{30}]^{4-}$.[22,26] Meanwhile, the as-prepared $Au_{12}Ag_{32}(SR)_{30}$@ZIF-8 composite displays excellent catalytic performance in CO_2 conversion under mild conditions.

Results and Discussion

The systematic approach to fabricating APNCs@MOFs is shown in **Scheme 1**. Taking $Au_{12}Ag_{32}(SR)_{30}$@ZIF-8 as an example, the complete fabrication includes two self-assembly processes: First, $[Au_{12}Ag_{32}(SR)_{30}]^{4-}$ nanoclusters with negative charges were prepared, followed by mixing with Zn^{2+} ions in methanol. The $[Au_{12}Ag_{32}(SR)_{30}]^{4-}$ nanoclusters quickly assembled with positively charged Zn^{2+} by electrostatic attraction. Subsequently, the solution of ZIF-8 precursors of 2-Methylimidazole (2-MeIM) in methanol was slowed poured into the above solution and mixed together. Finally, the $Au_{12}Ag_{32}(SR)_{30}$@ZIF-8 composite was obtained at room temperature without stirring for 24 h. To the best of our knowledge, this is the first report on the rational encapsulation of oil-soluble APNCs into MOFs by the "bottle-around-ship" method.

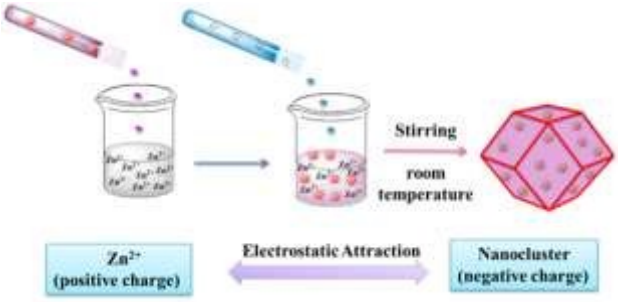

Scheme 1. Schematic illustration showing the rational encapsulation of APNCs@MOFs by Electrostatic Attraction.

The as-obtained $Au_{12}Ag_{32}(SR)_{30}$@ZIF-8 composite was characterized by XPS, UV-vis, FT-IR and XRD analyses (**Fig. 1**). First, we employed XPS analysis to confirm the existence of $[Au_{12}Ag_{32}(SR)_{30}]^{4-}$ and ZIF-8 in the $Au_{12}Ag_{32}(SR)_{30}$@ZIF-8 composite. The XPS result confirmed the existence of Au, Ag, Zn and S in the composite (**Fig. 1A**). The UV-vis spectra of fresh $[Au_{12}Ag_{32}(SR)_{30}]^{4-}$ nanoclusters and the supernatant of $[Au_{12}Ag_{32}(SR)_{30}]^{4-}$ + Zn^{2+} + 2-MeIM were also measured (Fig. 1B). The purified $[Au_{12}Ag_{32}(SR)_{30}]^{4-}$ nanoclusters showed two prominent peaks at 390 and 490 nm. The optical spectra were similar before and after mixing $Au_{12}Ag_{32}(SR)_{30}^{4-}$ with Zn^{2+}, and 2-MeIM, demonstrating that the $[Au_{12}Ag_{32}(SR)_{30}]^{4-}$ nanoclusters remains unchanged during the self-assembly process (**Fig. 1B**). To further confirm that $[Au_{12}Ag_{32}(SR)_{30}]^{4-}$ remains the structural integrity after attachment to MOFs, we treated the $Au_{12}Ag_{32}(SR)_{30}$@ZIF-8 composite with an acetic acid solution (pH = 4) to dissolve the ZIF-8 and extract the confined $[Au_{12}Ag_{32}(SR)_{30}]^{4-}$ nanoclusters. No spectral change was observed for the $[Au_{12}Ag_{32}(SR)_{30}]^{4-}$ nanoclusters (**Fig. 1B**), hence, $[Au_{12}Ag_{32}(SR)_{30}]^{4-}$ remains unchanged throughout the uptake/release process. Subsequently, we used FT-IR spectroscopy to further verify the formation of $Au_{12}Ag_{32}(SR)_{30}$@ZIF-8 composite. From **Fig. 1D**, one can see clearly that most peaks of the $Au_{12}Ag_{32}(SR)_{30}$@ZIF-8, including those at 2928 cm^{-1}, 1589 cm^{-1}, 1176 cm^{-1}, 756 cm^{-1} and 689 cm^{-1}, were from ZIF-8. Other peaks (at 1496 cm^{-1} and 771cm^{-1}) were benzene skeleton vibrational peaks and the adjacent di-substituted characteristic peaks, which were assigned to the protecting ligand $SPhF_2$ of $[Au_{12}Ag_{32}(SR)_{30}]^{4-}$ nanoclusters (**Fig. 1C**). Finally, the $Au_{12}Ag_{32}(SR)_{30}$@ZIF-8 nanocomposite was characterized by XRD (**Fig. 1D**). All the diffraction peaks of the $Au_{12}Ag_{32}(SR)_{30}$@ZIF-8 nanocomposite perfectly overlapped with those of the ZIF-8, indicating that ZIF-8 retained its crystalline phase structure after in situ growth with the APNCs encapsulated. On a note, the diffractions associated with Au and Ag were not observed due the ultrasmall size of $[Au_{12}Ag_{32}(SR)_{30}]^{4-}$ (i.e. significantly weakened diffraction). Summarizing the data obtained from FT-IR, UV-vis, XPS and XRD analyses, we can conclude that the $Au_{12}Ag_{32}(SR)_{30}$@ZIF-8 composite consists of intact $[Au_{12}Ag_{32}(SR)_{30}]^{4-}$ nanoclusters and ZIF-8. The Brunauer-Emmett-Teller (BET) surface area of $Au_{12}Ag_{32}(SR)_{30}$@ZIF-8 are determined to be 1528.7 m^2/g. For further confirming the position of the $[Au_{12}Ag_{32}(SR)_{30}]^{4-}$ nanoclusters, we analyzed the N_2 absorption–desorption isothermal and pore size distributions of $Au_{12}Ag_{32}(SR)_{30}$@ZIF-8 with comparation with ZIF-8 **(Fig. S1)**. Although the surface area of $Au_{12}Ag_{32}(SR)_{30}$@ZIF-8 composites decreased slightly in comparison with that of pure ZIF-8 (1643.0 m^2/g),[23] $Au_{12}Ag_{32}(SR)_{30}$@ZIF-8 and ZIF-8 have the similar isothermal features and pore diameter. In this condition, $[Au_{12}Ag_{32}(SR)_{30}]^{4-}$ nanoclusters are inserted as multi-functional scaffolds rather than embedded into the pores of ZIF-8. The results are similar to those reported in the literature.[18]

The morphology and composition of the $Au_{12}Ag_{32}(SR)_{30}$@ZIF-8 nanocomposite were characterized by scanning electron microscopy (SEM), transmission electron microscopy (TEM), high angle annular dark field-scanning

transmission electron microscope (HAADF-STEM), and energy dispersive X-ray spectroscopy (EDX). The SEM image shows that the $Au_{12}Ag_{32}(SR)_{30}$@ZIF-8 composite is of uniform rhombic dodecahedral shape (**Fig. S2**). HAADF-STEM and TEM images further confirmed that the uniform $[Au_{12}Ag_{32}(SR)_{30}]^{4-}$ nanoclusters are fully encapsulated in the ZIF-8 matrix with good dispersity (**Fig. 2A and 2B**). Unencapsulated $[Au_{12}Ag_{32}(SR)_{30}]^{4-}$ nanoclusters were not observed, indicating excellent encapsulation of nanoclusters. Energy-dispersive X-ray (EDX) spectroscopy element mapping was explored to further investigate the distribution of $[Au_{12}Ag_{32}(SR)_{30}]^{4-}$ nanoclusters. The elemental maps of Zn, N, Ag, Au and S of $Au_{12}Ag_{32}(SR)_{30}$@ZIF-8 are shown in **Fig. 3**, along with the STEM image and EDX spectrum. From the element mapping, it could be clearly seen that $[Au_{12}Ag_{32}(SR)_{30}]^{4-}$ nanoclusters are uniformly dispersed in the ZIF-8 matrix. Therefore, the strategy of introducing anionic $[Au_{12}Ag_{32}(SR)_{30}]^{4-}$ for subsequent ZIF-8 growth is demonstrated to be very successful based on electrostatic attraction.

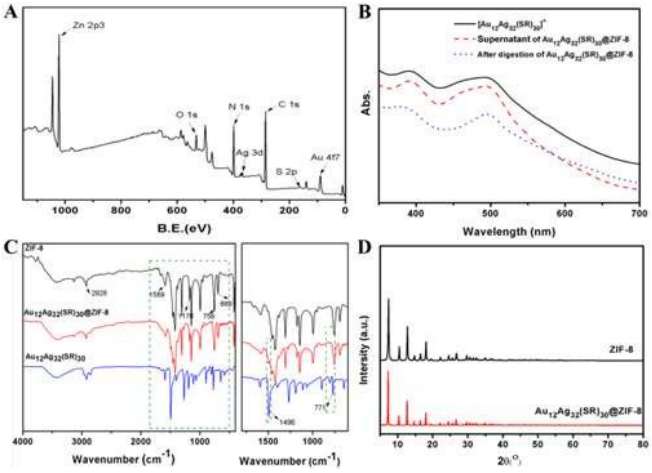

Fig. 1. The characteristic of $Au_{12}Ag_{32}(SR)_{30}$@ZIF-8. (A) XPS pattern of the $Au_{12}Ag_{32}(SR)_{30}$@ZIF-8 composite; (B) UV-vis spectra of $[Au_{12}Ag_{32}(SR)_{30}]^{4-}$, the supernatant after impregnation over Zn^{2+}+2-MeIM, and the solution after digesting the $Au_{12}Ag_{32}(SR)_{30}$@ZIF-8 composite; (C) FT-IR spectra of $[Au_{12}Ag_{32}(SR)_{30}]^{4-}$, ZIF-8 and $Au_{12}Ag_{32}(SR)_{30}$@ZIF-8; (D) XRD patterns of ZIF-8 and $Au_{12}Ag_{32}(SR)_{30}$@ZIF-8.

To confirm the effectiveness and importance of electrostatic attraction between $[Au_{12}Ag_{32}(SR)_{30}]^{4-}$ and Zn^{2+} of ZIF-8, we performed a control experiment using the cationic $[Au_{24}Ag_{46}(SR)_{32}]^{2+}$ nanoclusters[27] instead of the anionic $[Au_{12}Ag_{32}(SR)_{30}]^{4-}$ nanocluster, which $[Au_{24}Ag_{46}(SR)_{32}]^{2+}$ nanoclusters was structurally characterized by UV-vis spectrum (**Fig. S3**). In the obtained product, only a few $[Au_{24}Ag_{46}(SR)_{32}]^{2+}$ nanoclusters per MOF crystal were observed to be adsorbed on the outer surfaces of the crystals, while the majority of cationic nanoclusters remained free (**Fig. 2C**). This control experiment implies that the charge interaction between the APNCs and Zn^{2+} plays a critical role.

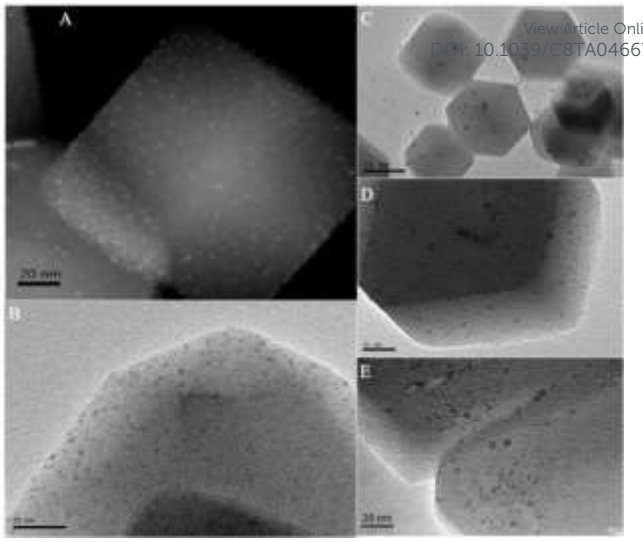

Fig. 2. (A) HAADF-STEM image of the $Au_{12}Ag_{32}(SR)_{30}$@ZIF-8 composite; (B)TEM images of the $Au_{12}Ag_{32}(SR)_{30}$@ZIF-8 composite; (C) the $Au_{24}Ag_{46}(SR)_{32}$@ZIF-8 composite; (D) the $Ag_{44}(SR)_{30}$@ZIF-8 composite; (E) the $Ag_{12}Cu_{28}(SR)_{30}$@ZIF-8 composite.

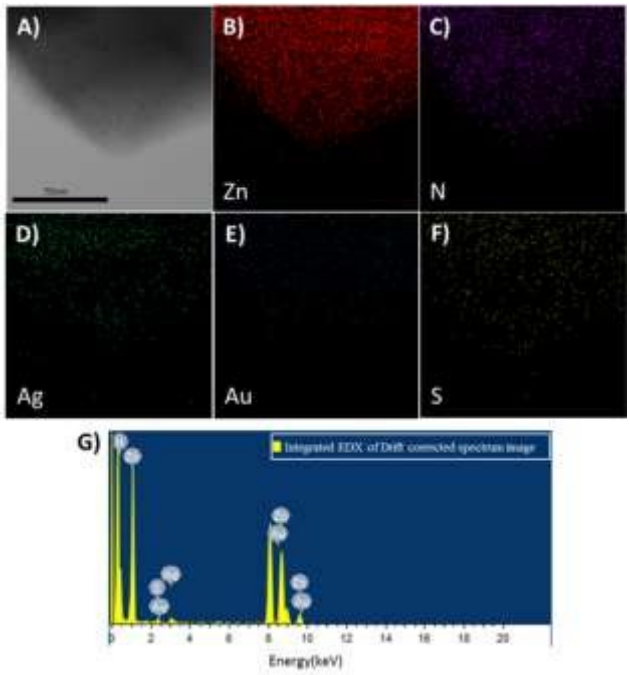

Fig. 3. STEM images and EDX spectrum of the $Au_{12}Ag_{32}(SR)_{30}$@ZIF-8 composite. (A) STEM images of the $Au_{12}Ag_{32}(SR)_{30}$@ZIF-8 composite; (B-F) Elemental maps of $Au_{12}Ag_{32}(SR)_{30}$@ZIF-8 composite Zn (B), N (C), Ag (D), Au (E), S (F); (G) EDX spectrum of the $Au_{12}Ag_{32}(SR)_{30}$@ZIF-8 composite.

We found that the electrostatic attraction strategy could be extended to other anionic APNCs. For example, $Ag_{44}(SR)_{30}$@ZIF-8 and $Ag_{12}Cu_{28}(SR)_{30}$@ZIF-8 were successfully prepared using the same strategy (**Fig. 2D and 2E, Fig. S2, Fig S4**). At the same time, the synthetic strategy presented here has also been proven to be effective with other MOF materials, such as ZIF-67 and MNHF. The corresponding hybrid materials $Au_{12}Ag_{32}(SR)_{30}$@ZIF-67, $Ag_{44}(SR)_{30}$@ZIF-67, $Ag_{12}Cu_{28}(SR)_{30}$@ZIF-67, $Au_{12}Ag_{32}(SR)_{30}$@MHCF and $Ag_{12}Cu_{28}(SR)_{30}$@MHCF were all successfully achieved and

View Article Online
DOI: 10.1039/C8TA04667K

structurally characterized by the FT-IR, UV-vis, XRD, SEM and TEM analyses, respectively (**Fig. S5-S11**). The synthesis method in this report truly achieved intact APNCs are well dispersed and fully encapsulated within the corresponding MOF crystallite based on these analysis results.

It is well known that utilizing renewable resources is an effective way to solve the increasingly serious environmental problems. Carbon dioxide (CO_2) is the easiest resource to obtain, which has advantages of being non-toxic, renewable, and inexpensive. However, few commercial run utilize CO_2 as a renewable feedstock because CO_2 is a thermodynamically stable and unreactive molecule. It is noteworthy that MOFs with Lewis acid centers as the active sites were exploited for the chemical fixation CO_2 in previous research.[14] In addition, Ag NPs@MOF composites were reported as highly effective catalysts for conversion of CO_2 to carbonyl compounds such as phenylpropiolic and carbonate ester.[14,15] Here, the accessibility of $Au_{12}Ag_{32}(SR)_{30}$@ZIF-8 composite, which combines the catalytic properties of $Au_{12}Ag_{32}(SR)_{30}$ nanoclusters and the CO_2 fixation capability of the ZIF-8 support, is first examined in the carboxylation of phenylacetylene as a model system (**Table 1**). The loading of $[Au_{12}Ag_{32}(SR)_{30}]^{4-}$ in the composite is 0.94 wt% determined by the inductively coupled plasma (ICP) analysis. Our initial studies focused on examining the catalytic performances for generation of 3-phenylpropiolic acid at various conditions, including different bases, solvents and catalysts. As expected, up to 100% yield was obtained by using $Au_{12}Ag_{32}(SR)_{30}$@ZIF-8 for the carboxylation reaction under mild conditions (0.24 equiv. Cs_2CO_3 or K_2CO_3, 1 atm CO_2, 60 mg catalyst and 50 °C in DMSO) (**Table 1, entries 3 and 4**). The TON (moles of product per mole of nanocluster) reaches up to 18164 for $Au_{12}Ag_{32}(SR)_{30}$@ZIF-8, which is far exceeding those of previous heterogeneous catalytic systems such as Ag@MIL-101 (36),[15] Ag@P-NHC (327),[28] Ag@Shiff-SiO_2 (705)[29] and $Pd_{0.2}Cu_{0.8}$/MIL-101 (691)[30] under similar catalytic reaction conditions (**Table S1**). Among various solvents, DMSO is found to be most effective in our system because DMSO is not only a good solvent for Cs_2CO_3 or K_2CO_3 but also a good solvent for CO_2,[31] which is consistent with the results of a previous report.[30, 32] It is also noteworthy that our catalytic system only used a slight amount of base (0.24 equiv), while an excess of base (> 1.2 equiv) was necessary in the reported systems.[14,15,28-30] Thus, our system has practical advantages over other approaches with bases in excess.

Table 1. Synthesis of phenylpropiolic acid from CO_2 and phenylacetylene with catalysts.[a]

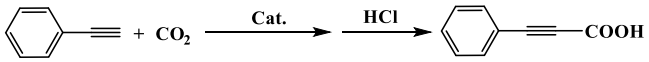

Entry	Cat	Solvent	Base	Yield(%)[b]	TON[c]
1	ZIF-8	DMSO	K_2CO_3	51.8	9420
2	$Au_{12}Ag_{32}(SR)_{30}$/CNTs	DMSO	K_2CO_3	50.7	9223
3	$Au_{12}Ag_{32}(SR)_{30}$@ZIF-8	DMSO	K_2CO_3	100	18164
4	$Au_{12}Ag_{32}(SR)_{30}$@ZIF-8	DMSO	Cs_2CO_3	100	18164
5	$Au_{12}Ag_{32}(SR)_{30}$@ZIF-8	DMSO	Na_2CO_3	25.8	4693
6	$Au_{12}Ag_{32}(SR)_{30}$@ZIF-8	DMF	K_2CO_3	12.7	2310
7	$Au_{12A}g_{32}(SR)_{30}$@ZIF-8	ToL	K_2CO_3	12.4	2256
8	$Au_{12}Ag_{32}(SR)_{30}$@ZIF-8	CH_3CN	K_2CO_3	8.9	1619

[a] Reaction conditions: phenylacetylene (1.0 mmol), 60 mg catalyst (0.94 wt. % loading of $[Au_{12}Ag_{32}(SR)_{30}]^{4-}$, 5.50×10^{-5} mol), base (0.24 mmol), CO_2 (1.0 atm), 50 ℃, solvent (1 mL), 24 h. [b] Yield of isolated product. [c] TON = (moles of product) / (moles of nanoclusters in the catalyst)

Moreover, the reaction was conducted by using plain ZIF-8 crystals and carbon nanotube-suppored $[Au_{12}Ag_{32}(SR)_{30}]^{4-}$ ($Au_{12}Ag_{32}(SR)_{30}$/CNTs) as catalysts for comparation under the above optimized conditions. Both showed lower catalytic activity under the same conditions, affording 51.8% and 50.7% yield of 3-phenylpropiolic acid, respectively (**Table 1, entries 1 and 2**). Based on the above results, the significantly enhanced catalytic activities of $Au_{12}Ag_{32}(SR)_{30}$@ZIF-8 was endowed by the synergistic effect of $[Au_{12}Ag_{32}(SR)_{30}]^{4-}$ and ZIF-8. For illustrating the ability of ZIF-8 support to fix and activate CO_2, we measured the CO_2 adsorption-desorption isotherms and FT-IR spectra. From **Fig. S12**, the absorptive capacity of CO_2 reached 20.96 and 10.72 mg/g (at 273 K) for ZIF-8 and $Au_{12}Ag_{32}(SR)_{30}$@ZIF-8, respectively, ensuring the possibility for the subsequent CO_2 transformation. The decrease in the amount of CO_2 uptake by $Au_{12}Ag_{32}(SR)_{30}$@ZIF-8 in comparison with ZIF-8 is attributed to the encapsulation of the $[Au_{12}Ag_{32}(SR)_{30}]^{4-}$ into the pores of ZIF-8. From **Fig. S13**, a

View Article Online
DOI: 10.1039/C8TA04667K

distinct absorption peak was observed at 1647 cm^{-1} in ZIF-8+CO_2 infrared spectrum, which should be assigned to the C=O stretching vibration of a specie generated from Zn^{2+} and CO_2 result from the fact that the signal was absent in ZIF-8. So, it is evident that CO_2 could be fixed and activated by ZIF-8 to form CO_2-Zn(2-MeIM)$_n$ complexes. To further elucidate the effect of encapsulated $[Au_{12}Ag_{32}(SR)_{30}]^{4-}$ nanoclusters, we investigatied the FT-IR spectra of phenylacetylene + $[Au_{12}Ag_{32}(SR)_{30}]^{4-}$, phenylacetylene and $[Au_{12}Ag_{32}(SR)_{30}]^{4-}$, respectively (**Fig. S14**). For phenylacetylene + $[Au_{12}Ag_{32}(SR)_{30}]^{4-}$, phenylacetylene was joined into the $[Au_{12}Ag_{32}(SR)_{30}]^{4-}$ nanoclusters (in DMSO solution) in the presence of K_2CO_3 under N_2 atmosphere at 50 °C for 4h, which is similar to the reaction conditions in this work. In sharp contrast with phenylacetylene, on the surface of deprotonation and coordination with the $[Au_{12}Ag_{32}(SR)_{30}]^{4-}$ nanoclusters, the ≡C-H stretching (3293 cm^{-1}) disappear (the 3500 cm-1 broad band likely originated from H_2O) and the C≡C stretching downshifts from 2113 cm^{-1} to 2098 cm^{-1}. It is therefore that phenylacetylene and $[Au_{12}Ag_{32}(SR)_{30}]^{4-}$ nanocluster coordinated to form a Ph-C≡C---$Au_{12}Ag_{32}(SR)_{30}$ intermediate, leading to lowing the C≡C bonding order.

Interestingly, the $Au_{12}Ag_{32}(SR)_{30}$@ZIF-8 composite maintains its high activity in the five consecutive catalytic runs (**Fig. S15**). The results clearly demonstrate that $Au_{12}Ag_{32}(SR)_{30}$@ZIF-8 composite shows robust stability and recyclability as a heterogeneous catalyst for the CO_2 transformation to propiolic acids. The structure and composition of recycled $Au_{12}Ag_{32}(SR)_{30}$@ZIF-8 were almost the same as those of the fresh catalyst, evidenced by the TEM image, UV-Vis spectrum, FT-IR and XRD pattern (**Fig. S16**). Under optimization of the reaction conditions, various alkyne substrates were subjected to this carboxylation reaction (0.24 equiv K_2CO_3, 1 atm CO_2, DMSO, 50°C). From **Table 2**, it is obvious that $Au_{12}Ag_{32}(SR)_{30}$@ZIF-8 catalyst was very effective for terminal alkynes. These substrates are transferred to the corresponding products in satisfactory yields. The substrates with electron donating groups on aryl groups gave rise to higher yields than those with electron withdrawing groups (**Table 2, entries 1–4**). When ethynylcyclopropane was used as an alkyl acetylene substrate, the reaction also proceeded smoothly and the yield of desired 3-cyclopropylpropiolic acid can reach 89.8% (**Table 2, entry 5**).

In general, $Au_{12}Ag_{32}(SR)_{30}$@ZIF-8 catalyzed carboxylation reactions of both aryl- and alkyl- terminal alkynes with CO_2. Based on the above results and the literature reports,[15,29,33] we rationalized a possible mechanism for our catalytic system (**Scheme 2**). First, $[Au_{12}Ag_{32}(SR)_{30}]^{4-}$ nanocluster activates the terminal alkyne with base to form a Ph-C≡C---$Au_{12}Ag_{32}(SR)_{30}$ intermediate I; Meanwhile, CO_2 is fixed and activated by ZIF-8 to generate an intermediate CO_2-Lewis acid complex II. The activated CO_2 would then be inserted into the nearby M–C bond to generate the carboxylate III. Following the product formation, the intermediate I is regenerated by metathesis with alkyne. The synergistic effect between the $[Au_{12}Ag_{32}(SR)_{30}]^{4-}$ nanocluster and ZIF-8 enormously enhanced the catalytic activity of our hybrid system.

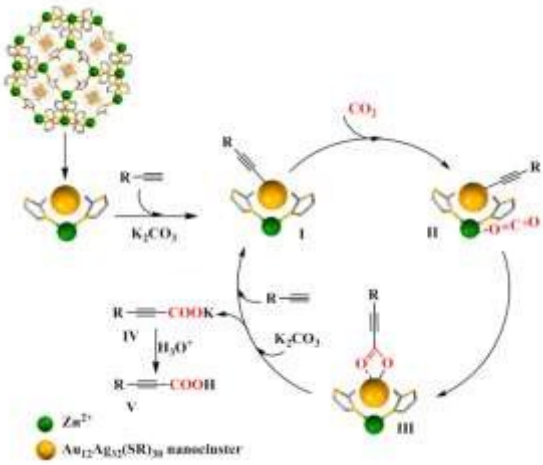

Scheme 2. Proposed reaction mechanism toward CO_2 and phenylacetylene over $Au_{12}Ag_{32}(SR)_{30}$@ZIF-8.

Table 2. Synthesis of phenylpropiolic acid by $Au_{12}Ag_{32}(SR)_{30}$@ZIF-8.[a]

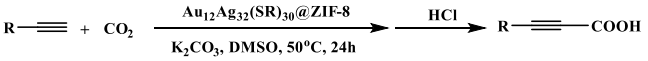

Entry	Alkyne	Product	Yield(%)[b]	TON[c]
1	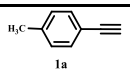 1a	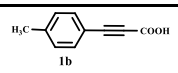 1b	97.4	17719
2	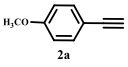 2a	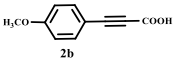 2b	99.6	18119
3	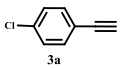 3a	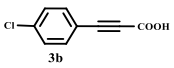 3b	92.2	16773
4	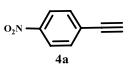 4a	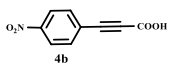 4b	79.0	14371
5	 5a	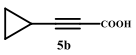 5b	89.8	16263

[a] Reaction conditions: various alkyne (1.0 mmol), 60 mg catalyst (0.94 wt % $Au_{12}Ag_{32}(SR)_{30}^{4-}$ loading, 5.50 × 10^{-5} mol), K_2CO_3 (0.24 mmol), CO_2 (1.0 atm), 50℃, DMSO (1 mL), 24 h. [b] Yield of isolated product. [c] TON = (moles of product) / (moles of nanoclusters in the catalyst).

Conclusion

In conclusion, we have established an "Electrostatic Attraction Strategy" to create new types of APNCs@MOFs in a controllable way, which provide ideal candidates for the study of structure-activity relationship due to their well-defined compositions and tunable structures of both components. The method is applicable to synthesis of various APNCs@MOFs catalysts including all the combinations of $[Au_{12}Ag_{32}(SR)_{30}]^{4-}$, $[Ag_{44}(SR)_{30}]^{4-}$, $[Ag_{12}Cu_{28}(SR)_{30}]^{4-}$ nanoclusters with ZIF-8, ZIF-67, MHCF frameworks. Moreover, the as-obtained $Au_{12}Ag_{32}(SR)_{30}$@ZIF-8 composite shows excellent performance in capturing CO_2 and converting phenylacetylene into phenylpropiolate under mild conditions (50 ^{o}C and ambient CO_2 pressure), which encompass the benefits of porous and molecular sieving behavior characterized by the MOF matrix together with the functional behavior characteristic of APNCs. The promising APNCs@MOFs materials are also expected to find wide applications in the synthesis of fine chemicals.

Conflicts of interest

There are no conflicts to declare.

Acknowledgements

The work is supported by National Natural Science Foundation of China (21372006, U1532141, 21631001, 61601001), Natural Science Foundation of Education Department of Anhui Province (KJ2014A013, KJ2017A009, KJ2016A017), and 211 Project of Anhui University.

Notes and references

1. Q. Yang, Q. Xu and H. L. Jiang, *Chem. Soc. Rev.,* 2017, **46,** 4774-4808.
2. Y. Zhang, J. Guo, L. Shi, Y. Zhu, K. Hou, Y. Zheng and Z.Tang, *Sci. Adv.,* 2017, **3,** e1701162.
3. R. Ghorbani-Vaghei, D. Azarifar, S. Daliran and A. R. Oveisi, *RSC Adv.,* 2016, **6,** 29182-29189.
4. J. Yang, F. Zhang, H. Lu, X. Hong, H. Jiang, Y. Wu and Y. Li, *Angew. Chem. Int. Ed.,* 2015, **54,** 10889-10893.
5. H. K. Lee, C. S. L. Koh, Y. H. Lee, C. Liu, I. Y. Phang, X. Han, C-K. Tsung and X. Y. Ling, *Sci. Adv.,* 2018, **4,** eaar3208.
6. L. Tao, C.Y. Lin, S. Dou, S. Feng, D. Chen, D. Liu, J. Huo, Z. Xia and S. Wang, *Nano Energy,* 2017, **41,** 417-425.
7. J. Liang, R. P. Chen, X. Y. Wang, T. T. Liu, X. S. Wang, Y. B. Huang and R. Cao, *Chem. Sci.,* 2017, **8,** 1570-1575.
8. J. Xu, R. Sinelnikov and Y. Huang, *Langmuir,* 2016, **32,** 5468-5479.
9. D. Wang, R. Huang, W. Liu, D. Sun and Z. Li, *ACS Catal.,* 2014, **4,** 4254-4260.
10. F. Vermoortele, R. Ameloot, A. Vimont, C. Serre and D. De Vos, *Chem. Commun.,* 2011, **47,** 1521-1523.
11. A. Dhakshinamoorthy, A. M. Asiri and H. Garcia, *ACS Catal.,* 2017, **7,** 2896-2919.
12. B. An, J. Zhang, K. Cheng, P. Ji, C. Wang and W. Lin, *J. Am. Chem. Soc.,* 2017, **139,** 3834-3840.
13. Z. Guo, C. Xiao, R. V. Maligal-Ganesh, L. Zhou, T. W. Goh, X. Li, D. Tesfagaber, A. Thiel and W. Huang, *ACS Catal.,* 2014, **4,** 1340-1348.
14. N. N. Zhu, X. H. Liu, T. Li, J. G. Ma, P. Cheng and G. M. Yang, *Inorg. Chem.,* 2017, **56,** 3414-3420.
15. X. H. Liu, J. G. Ma, Z. Niu, G. M. Yang and P. Cheng, *Angew. Chem. Int. Ed.,* 2015, **54,** 988-991.
16. L. Liu, Y. Song, H. Chong, S. Yang, J. Xiang, S. Jin, X. Kang, J. Zhang, H. Yu and M. Zhu, *Nanoscale, 2016,* **8,** 1407-1412.
17. C. Liu, C. J. Zeng, T. Y. Luo, A. D. Merg, R. C. Jin and N. L. Rosi, *J. Am. Chem. Soc.,* 2016, **138**, 12045–12048.
18. Y. Luo, S. Fan, W. Yu, Z. Wu, D. A. Cullen, C. Liang, J. Shi and C. Su, *Adv. Mater.,* 2017, **30,** 1704576.
19. X. Zhou, Y. X. Yin, L. J. Wan and Y. G. Guo, *Adv. Energy Mater.,* 2012, **2,** 1086-1090.
20. J. Yang, J. W. Kim and H. S. Shin, *Adv. Mater.,* 2012, **24,** 2299-2303.
21. K. L. Niece, J. D. Hartgerink, J. J. J. M. Donners and S. I. Stupp, *J. Am. Chem. Soc.,* 2003, **125,** 7146-7147.
22. H. Yang, Y. Wang, H. Huang, L. Gell, L. Lehtovaara, S. Malola, H. Hakkinen and N. Zheng, *Nature commun.,* 2013, **4,** 2422.
23. G. Lu, S. Li, Z. Guo, O. K. Farha, B. G. Hauser, X. Qi, Y. Wang, X. Wang, S. Han, X. Liu, J. S. DuChene, H. Zhang, Q. Zhang, X. Chen, J. Ma, S. C. Loo, W. D. Wei, Y. Yang, J. T. Hupp and F. Huo, Nature Chem., 2012, 4, 310-316.
24. X. Ge, Z. Li and L. Yin, *Nano Energy,* 2017, **32,** 117-124.
25. H. Pang, Y. Zhang, T. Cheng, W. Y. Lai and W. Huang, *Nanoscale,* 2015, **7,** 16012-16019.
26. J. Yan, H. Su, H. Yang, C. Hu, S. Malola, S. Lin, B. K. Teo, H. Hakkinen and N. Zheng, *J. Am. Chem. Soc.,* 2016, **138,** 12751-12754.
27. S. Wang, S. Jin, S. Yang, S. Chen, Y. Song, J. Zhang and M. Zhu, *Sci. Adv.,* 2015, **1,** e1500441.
28. D. Yu, M. X. Tan and Y. Zhang, *Adv. Synth. Catal.,* 2012, **354,** 969-974.
29. Z. Wu, L. Sun, Q. Liu, X. Yang, X. Ye, Y. Hu and Y. Huang, *Green Chem.,* 2017, **19,** 2080-2085.
30. M. Trivedi, Bhaskaran, A. Kumar, G. Singh, A. Kumar and N. P. Rath, *New J. Chem.,* 2016, **40,** 3109-3118.
31. A. Gennaro, A. A. Isse and E. Vianello, *J. Electroanal, J. Electroanai. Chem*., 1990, **289,** 203-215.
32. Z. Wu, Q. Liu, X. Yang, X. Ye, H. Duan, J. Zhang, B. Zhao and Y. Huang, *ACS Sustainable Chem. Eng.,* 2017, **5,** 9634-9639.
33. R. A. Molla, K. Ghosh, B. Banerjee, M. A. Iqubal, S. K. Kundu, S. M. Islam, A. Bhaumik, *J. Colloid Interf. Sci.,* 2016, **477**, 220–229.

View Article Online
DOI: 10.1039/C8TA04667K

Table of contents

The composites APNCs@MOFs have been successfully synthesized by electrostatic attraction strategy, which served as excellent catalysts for converting CO_2.